Single step combustion synthesized Cu/$Ce_{0.8}Zr_{0.2}O_2$ for methanol steam reforming: structural insights from *in situ* XPS and HRTEM studies

Dipak Das[1], Jordi Llorca[2], Montserrat Dominguez[2], and Arup Gayen*[1]

[1]Department of Chemistry, Jadavpur University, Kolkata 700032, India
[2]Institut de Tècniques Energètiques and Centre for Research in Nanoengineering, Universitat Politècnica de Catalunya, 08028 Barcelona, Spain

Abstract Single step combustion synthesized Cu (5–15 at.-%)/$Ce_{0.8}Zr_{0.2}O_2$ materials containing highly dispersed copper have been assessed for methanol steam reforming (MSR). The activity patterns suggest Cu (10 at.-%)/$Ce_{0.80}Zr_{0.20}O_2$ as the most active formulation, converting ~51% methanol at 300 °C at a gas hourly space velocity of 40,000 h^{-1} (W/F = 0.09 s). The *in situ* XPS experiments carried over the most active sample show a sharp falloff of Cu-surface concentration from a considerably high value of 26% before to 7.4% after the *in situ* MSR tests and it is associated with the complete reduction of oxidized Cu-species (Cu^{2+}) to metallic copper (Cu^0). These findings point to the sintering of copper during MSR which is attributed to be responsible for the deactivation observed with time on stream. Interestingly, the MSR activity is shown to be regenerated nearly completely through an intermediate *in situ* oxidation step in the consecutive cycles of methanol reforming.

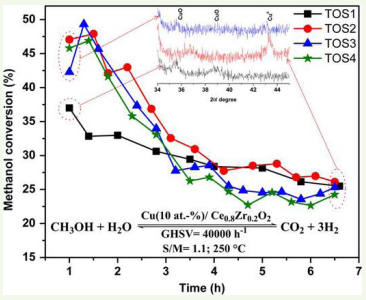

Keywords Copper, Ceria–zirconia, Solution combustion, Methanol steam reforming, Cu-sintering, Regeneration
Cite this article D. Das, J. Llorca, M. Dominguez and A. Gayen: Catal. Struct. React., 2015, 1, 174–182

Introduction

Hydrogen energy is proven to be a promising alternative to fossil fuels. The most potential environment-friendly technology for the production of clean electrical power can be developed by the help of hydrogen-powered fuel cells.[1] The on-board reforming of hydrocarbons has gained renewed interest of researchers as it allows hydrogen production *in situ*, which can solve the problems of storage.[2,3] The production of fuel cell grade hydrogen remains a challenging issue. The low temperature methanol steam reforming (MSR) is a simple and convenient route to produce nearly CO-free hydrogen.[4]

The literature reports several Cu-based[5–9] and Pd-based[4,10] catalysts for MSR. The Cu-based catalysts are comparatively more active and selective at lower temperature. The commercially used MSR catalyst is Cu/ZnO/Al_2O_3 which contains a high loading of copper and ZnO and a relatively low amount of Al_2O_3.[11] The usefulness of ZnO and Al_2O_3 is due to several factors that are widely discussed in the literature.[12,13] But finding a suitable alternative to Al_2O_3 to increase the reducibility of copper is highly needed. Addition of ZrO_2 to Cu-based Al_2O_3-supported catalysts is shown to enhance the MSR activity.[14,15] It also increases the reducibility of CuO. On the other hand, CeO_2 improves the thermal stability of Al_2O_3-supported Cu-catalysts and it also reduces CO selectivity through the water gas shift (WGS) reaction.[16,17] The formation of CO from CO_2 occurs mainly via the reverse WGS reaction.[5,14,18,19] Whereas the Cu(111) model system is more selective toward CO_2 and H_2, the Pd(111) model system is more selective toward CO and H_2.[20] The nature of active site, particularly the oxidation state of copper is as debated as the mechanistic aspects. Nevertheless, there is a general consensus that the MSR activity depends very much on Cu^+ to Cu^0 molar ratio.[7,21,22]

There are limited literature reports on Cu-loaded ceria–zirconia for MSR activity. Mastalir *et al*. have shown long-term stability in MSR over a 15 mol % Cu-loaded CeO_2–ZrO_2 (1:1 mol ratio).[6] Oguchi *et al*. have reported a CuO/ZrO_2/CeO_2 catalyst (weight ratio of 8/1/1) which exhibits enhanced catalytic performance in MSR through stabilization of Cu_2O on the catalyst surface.[7] Pojanavaraphan *et al*. have established the beneficial effect of Au addition to Cu/$Ce_{0.75}Zr_{0.25}O_2$ for this reaction.[23,24] In a very recent report, we have studied the MSR behavior of copper impregnated over various Ce–Zr oxides.[25]

*Corresponding author, email: agayen@chemistry.jdvu.ac.in

Received 15 October 2015; accepted 8 December 2015
DOI 10.1080/2055074X.2015.1105616

In this work, we report the synthesis of Cu (5–15 at.-%)/$Ce_{1-x}Zr_xO_2$ with varied Ce to Zr molar ratio as catalyst materials for MSR via a single step solution combustion method. Two formulations, namely Cu (10 at.-%)/$Ce_{0.8}Zr_{0.2}O_2$ and Cu (15 at.-%)/$Ce_{0.8}Zr_{0.2}O_2$, have been thoroughly investigated. The MSR studies have also been carried out *in situ* and monitored by XPS.

Experimental

Preparation of materials

We have synthesized Cu-loaded $Ce_xZr_{1-x}O_2$ (x = 0.6, 0.7, and 0.8) solid solutions by a single step solution combustion method. In this method, the metal nitrate salts and an organic fuel taken in stoichiometric amounts are first dissolved in the minimum volume of double distilled water in a borosilicate dish through warming. The resulting solution is then transferred to a preheated muffle furnace maintained at the ignition temperature for combustion. Initially, the solution boils with frothing and foaming followed by complete dehydration when the surface gets ignited and burns to yield a solid product within few minutes.

Typically, the preparation of Cu (10 at.%)/$Ce_{0.8}Zr_{0.2}O_2$ involves combustion of 0.3060 g of $Cu(NO_3)_2{\cdot}3H_2O$ (Merck, GR, 99%), 5.0 g of $(NH_4)_2Ce(NO_3)_6$ (Merck, GR, 99%), and 0.5272 g of $ZrO(NO_3)_2{\cdot}H_2O$ (Loba Chemie, ZrO_2 assay >44.5%) with 3.007 g of oxalyl dihydrazide ($C_2H_6N_4O_2$, ODH) corresponding to the molar ratio of 0.10:0.72:0.18:2.01 dissolved in ~30 mL of double distilled water at ~350 °C. The ceria–zirconia oxides (with or without copper loading) exhibit flaming-type combustion and the combustion was completed within a minute. The color of the as-synthesized sample is gray.

Characterization of materials

The powder X-ray diffraction (XRD) data were collected on a Bruker D8 Advance X-ray diffractometer using Cu Kα radiation (λ = 1.5418 Å) generated at 40 kV and 40 mA. Data were collected in the 2θ range of 10–100° using a Lynxeye detector with 0.02° step size and scan time of 0.4 s per step and analyzed by ICDD (International Centre for Diffraction Data) database for phase identification. Average particle sizes were calculated from the line-broadening of the XRD peaks using the Scherrer equation.

The Brunauer-Emmett-Teller (BET) specific surface areas (SAs) were determined using nitrogen in an Autosorb 1 C SA analyzer (Quantachrome, USA). Prior to analysis, the samples were degassed at 250 °C in vacuum for 2 h.

High-resolution transmission electron microscopy (HRTEM) was performed at an accelerating voltage of 200 kV in a JEOL 2010F instrument equipped with a field emission source. The point-to-point resolution was 0.19 nm, and the resolution between lines was 0.14 nm. The magnification was calibrated against an Si standard. No induced damage of the samples was observed under prolonged electron beam exposure. Samples were dispersed in alcohol in an ultrasonic bath, and a drop of supernatant suspension was poured onto a holey carbon-coated grid. Images were not filtered or treated by means of digital processing, and they correspond to raw data.

X-ray photoelectron spectroscopy (XPS) surface characterization was done on a SPECS system equipped with an Al anode XR50 source operating at 150 mW and a Phoibos 150 MCD-9 detector. The analysis chamber was maintained at a pressure always below 10^{-7} Pa. The area analyzed was about 2 mm × 2 mm setting the pass energy of the hemispherical analyzer at 25 eV and the energy step at 0.1 eV. Charge stabilization was achieved by using a SPECS Flood Gun FG 15/40. The sample powders were pressed to self-consistent disks. The spectra were recorded in the following sequence: survey spectrum, C 1s, Cu 2p, Ce 3d, Zr 3d, Cu LMM Auger, and C 1s again to check for charge stability as a function of time and the absence of degradation of the sample during the analyses. The data processing was performed with the CasaXPS program (Casa Software Ltd., UK). The binding energy values have been centered using the u‴ peak of Ce 3d at 916.9 eV (because C 1s signal is partly masked by Ce 4s signal). The atomic fractions (%) were calculated using peak areas normalized on the basis of acquisition parameters after background subtraction, experimental sensitivity factors, and transmission factors provided by the manufacturer.

The *in situ* MSR experiments were performed in a reaction chamber connected to the XPS analysis chamber that allowed treatments up to 600 °C at atmospheric pressure and sample transfer without exposure to air. The temperature of the sample was measured with a thermocouple in contact with the sample holder, which was heated with an IR lamp. The evolution of products during the *in situ* experiments (0–100 amu) was followed by a mass spectrometer. Gases were introduced by means of mass flow controllers and liquids were introduced through bubbling the appropriate amount of carrier gas (Ar) to reach the required steam/methanol (S/M) ratio of 1.1 used in our experiments.

Test of reforming activity

The MSR was performed in a continuous-flow fixed-bed downflow quartz microreactor (ID = 6 mm) in the temperature range from 200 to 300 °C under atmospheric pressure. In each experiment, 0.1 g of sample (85–100 mesh) was placed on a bed of quartz wool in a vertical tube furnace. The temperature of the furnace was maintained by thyristor-powered Eurotherm PID controller (model 2416) and a K-type thermocouple (Omega) was inserted in the reactor in close contact with the catalyst bed to measure the actual reaction temperature. A premixed water (Millipore) and methanol (Spectrochem, 99.9%) solution (water/methanol = 1.1) was introduced by a KD100 syringe pump (Cole Parmer) at a rate of 0.4 mL h^{-1}. The liquid was passed through stainless steel tube and traveled a very short distance during which it was evaporated by heating tapes maintained at sufficiently high temperature (>150 °C) to ensure a single phase flow. Flow of nitrogen (23.5 mL min^{-1}) through the system was controlled precisely by Bronkhorst High-Tech B V thermal mass flow controller (model F-201CB). The samples were tested at a gas hourly space velocity (GHSV) of 40,000 h^{-1}. The product gases (e.g. CO, CO_2 and H_2) were analyzed by an online gas chromatograph, Agilent 7890A equipped with a polar Porapak Q and a molecular sieve 5 Å columns, and a thermal conductivity detector and a flame ionization detector (FID). To increase the sensitivity toward CO and CO_2, the FID is associated with a methanizer which converts these gases into CH_4 (though CH_4 was not detected in our experiments).

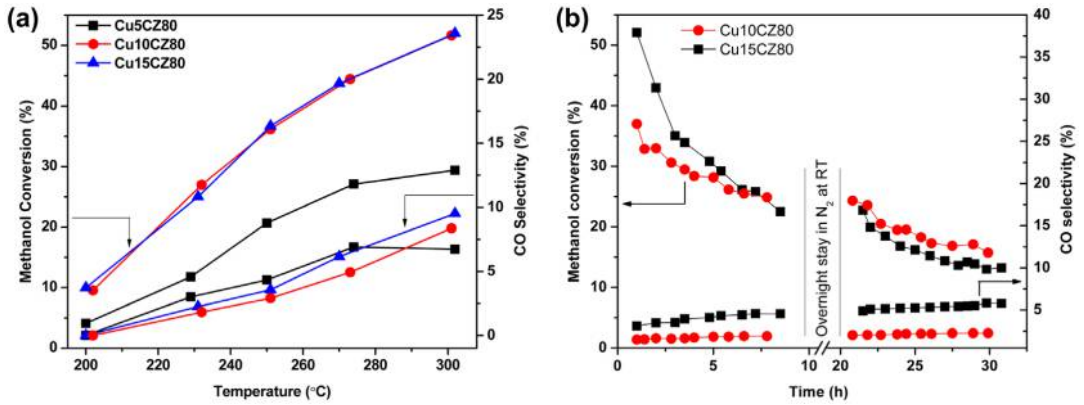

Figure 1 MSR behavior of combustion synthesized catalysts at GHSV of 40,000 h^{-1}: (a) effects of copper loading on CZ80 and (b) time-on-stream behavior of Cu10CZ80 and Cu15CZ80 catalysts at 250 °C (S/M = 1.1; balance is N_2 in each case)

Results and Discussion

Selection of materials

The preliminary MSR experiments (data not included here) carried out over 10 at.-% copper over the $Ce_{1-x}Zr_xO_2$ (Ce–Zr) supports with varied Ce/Zr molar ratio show the 10 at.-% Cu-loaded $Ce_{0.8}Zr_{0.2}O_2$ (named as CZ80), defined as Cu10CZ80, to be the most active formulation exhibiting ~51% methanol conversion at 300 °C at the GHSV of 40,000 h^{-1} (W/F = 0.09 s). It is to be noted that none of the pure Ce–Zr oxides show any MSR activity over the whole range of temperatures investigated. This indicates that the MSR activity reported here is due to the loading of copper on the Ce–Zr oxides.

Fig. 1*a* represents the effect of copper loading (5, 10 and 15 at.-%) on the MSR behavior of CZ80. As expected, the conversion of methanol is the lowest in the case of the lowest Cu-loaded sample, 5 at.-% Cu on CZ80 (designated as Cu5CZ80), which shows a conversion of 29% at 300 °C with the highest CO selectivity up to 275 °C. The methanol conversions recorded over Cu10CZ80 and the highest copper-containing sample, 15 at.-% Cu on CZ80 (represented as Cu15CZ80), are found to be similar. But the CO selectivity exhibited by the Cu15CZ80 catalyst is higher than recorded for the Cu10CZ80 catalyst in the complete range of temperatures. The activity behaviors of different Cu-loaded samples led us to choose Cu10CZ80 and Cu15CZ80 as the important formulations for further studies.

The BET-specific SA of the CZ80 oxide is 22 $m^2\ g^{-1}$. For the lower Cu-loaded sample, Cu10CZ80, the SA increases marginally to 25 $m^2\ g^{-1}$ and it remains similar to the support for the higher Cu-loaded sample Cu15CZ80. So, the presence of copper appears to have an insignificant role on the SA of the single step combustion synthesized catalysts.

Durability test

The time-on-stream (TOS) activity patterns of Cu10CZ80 and Cu15CZ80 samples at 250 °C (other reaction conditions remaining the same) were studied for a total of 20 h in two consecutive days leaving behind the catalyst overnight at room temperature (RT) in N_2. The conversion behaviors are shown in Fig. 1*b*. Both the samples show a continuous decrease in conversion with TOS. Though the Cu15CZ80 sample shows a higher conversion during the initial hours than exhibited by the Cu10CZ80 sample, it decreases rapidly to 22% within first 8 h and beyond that the TOS conversion profile of the Cu15CZ80 sample actually lies below that of the Cu10CZ80 sample exhibiting a methanol conversion of just 13% at the end of the test. On the contrary, the Cu10CZ80 catalyst exhibits an initial methanol conversion of ~36% at 250 °C that decreases to ~25% after 8 h and it is ~16% after 20 h (see Fig. 1*b*). Thus, the Cu10CZ80 is the best formulation made via the single step combustion route in this study.

A detailed surface analysis of the as-prepared Cu10CZ80 sample and the same obtained after *in situ* MSR reaction (at 300 °C, the temperature at which the sample showed the highest reforming activity) in the XPS reaction chamber was subsequently carried out in order to gain insight(s) about the change(s) in surface composition that prevails during MSR in the microreactor.

In situ XPS studies

Analysis of the XPS data revealed that the as-prepared sample has a surface atomic Ce/Zr ratio of 4, which is exactly the stoichiometric (theoretical) value corresponding to $Ce_{0.8}Zr_{0.2}O_2$. Approximately, the same ratio is recorded after MSR (Ce/Zr = 4.5). This indicates that the ceria–zirconia surface composition remains essentially unaffected apart from marginal cerium enrichment on the surface during the MSR tests.

Fig. 2*a* and *b* corresponds to the Cu 2p core level regions of Cu10CZ80 for the as-prepared sample and the sample after *in situ* MSR, respectively. These spectral features together with the respective Auger lines (see Fig. 2*c* and *d*) reveal that the as-prepared sample consists exclusively of oxidized copper (the $2p_{3/2}$ peaks at binding energies higher than 934 eV with characteristic satellite features correspond to Cu^{2+}). After MSR, the oxidized Cu-species transforms completely into metallic copper (the $2p_{3/2}$ peak at 932.4 eV is due to Cu^0, which is in accordance with the absence of satellite lines). The dispersion of Cu is impressively high in the as-prepared sample giving an atomic Cu/(Ce+Zr) ratio of about 26%, which is a value much higher than that expected for a 10 at.-% Cu loading. After MSR, the Cu/(Ce+Zr) ratio is calculated to be 7.4%, which means that the dispersion of Cu drops, probably by sintering.

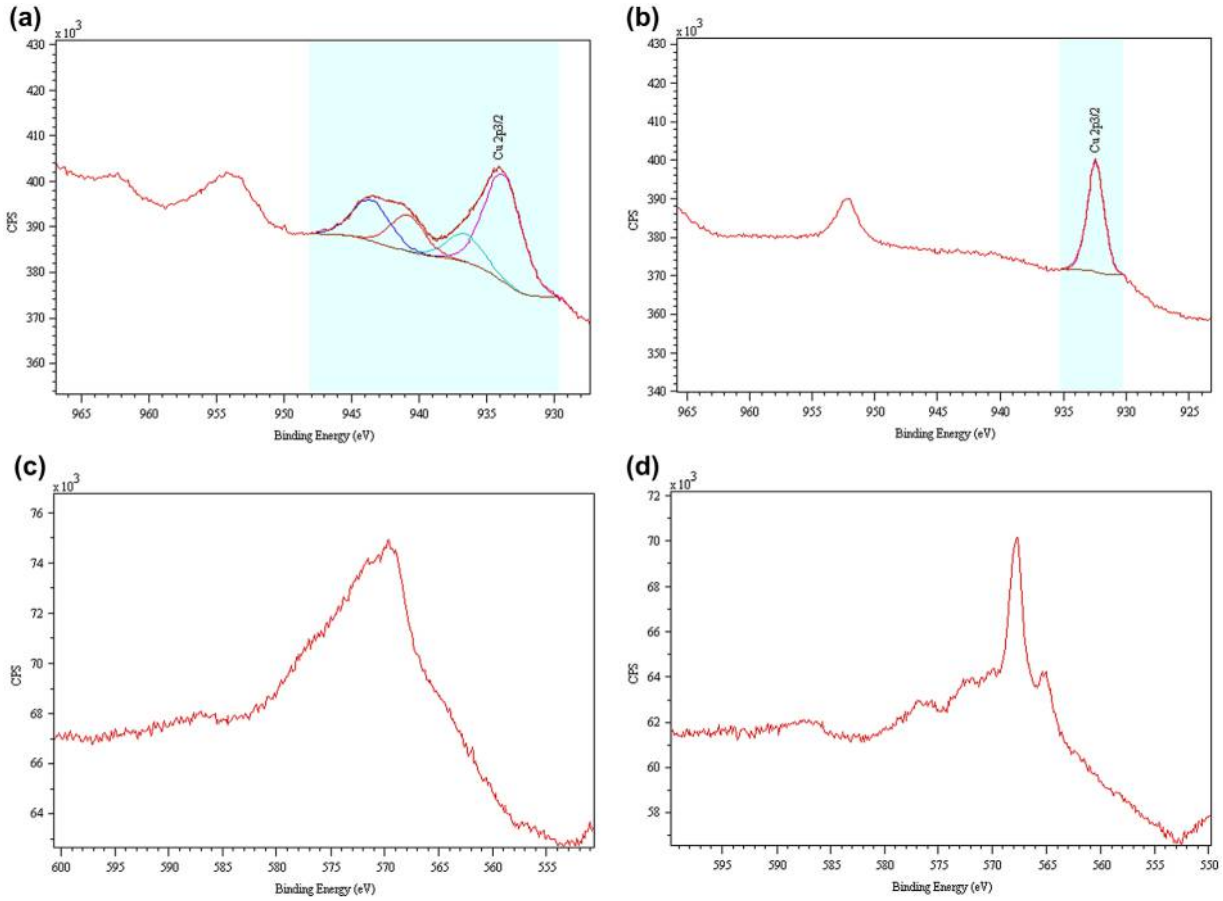

Figure 2 XPS of Cu 2p regions of (a) as prepared and (b) after MSR samples of Cu10CZ80; Cu LMM Auger spectra of (c) as prepared and (d) after MSR samples of Cu10CZ80.

This would explain the decay in catalytic activity during TOS reported above.

XRD studies

The powder XRD patterns of pure CZ80 and the three Cu-loaded CZ80 materials are shown in Fig. 3. All the peaks correspond to the cubic fluorite structure, as expected. The average size of the crystallites calculated using the Scherrer equation is ~22 nm. The peaks observed at 35.5° and 38.7° correspond to CuO(002) and CuO(111) planes in the as-synthesized materials. The intensity of these CuO-related peaks increases with the increase of Cu loading (see the inset of Fig. 3 for a better view). The CuO(111)/CeO_2(111) peak area ratio increases from 0.006 in Cu5CZ80 to 0.014 in Cu10CZ80 and 0.023 in Cu15CZ80. The least-square-refined lattice parameters of the pure CZ80 is 5.3687 (5) Å and those for the Cu-loaded oxides are 5.3719 (6) Å for Cu5CZ80, 5.378 (1) Å for Cu10CZ80, and 5.371 (1) for Cu15CZ80. After subtracting the $K\alpha_2$ contribution, the least-square-refined lattice parameters are calculated to be 5.372 (1) Å, 5.374 (1) Å, 5.378 (2) Å, and 5.3734 (3) Å, respectively, for the CZ80, Cu5CZ80, Cu10CZ80, and Cu15CZ80 samples. Thus, the lattice parameters of the Cu-loaded samples are marginally higher than that of the pure oxide and, taking into account that a decrease in lattice parameter is expected upon copper substitution [Ce^{4+} (0.097 nm), Ce^{3+} (0.1143 nm), Zr^{4+} (0.084 nm), and Cu^{2+} (0.073 nm)], it is difficult to comment conclusively about the presence or absence of substitutional Cu in the Ce–Zr solid solution phase. It appears that a large fraction of the copper is present as finely dispersed CuO nanoparticles and the rest minor fraction of copper may have the possibility to remain as interstitial punctual defects in the Ce–Zr lattice owing to the small size of the Cu^{2+} ion.[26]

HRTEM studies

Under low magnification (image not included), the CZ80 support is constituted by crystallites ranging from 10 to 50 nm. All the support particles are well crystallized, as shown in the lattice fringe image depicted in Fig. 4*a*. Considering the polycrystalline nature of the crystallites, the size range is consistent with the Scherrer size of 22 nm. Unlike the TEM with highly localized imaging, the information obtained from Scherrer's formula from the XRD data is the information from the bulk material. Thus, the particles size obtained by local imaging (HRTEM) will be averaged out using Scherrer's formula.[27]

Similar characteristics are encountered in the samples loaded with copper in their as-prepared forms, Cu10CZ80 and Cu15CZ80. A lattice fringe image of Cu10CZ80 is depicted in Fig. 4*b*. It should be stressed out that no copper-containing particles are recognized in the HRTEM images of the Cu10CZ80 catalyst, which suggest that copper may be incorporated into the support nanoparticles or it is so highly dispersed that it escapes TEM detection. Although the lattice fringes do not

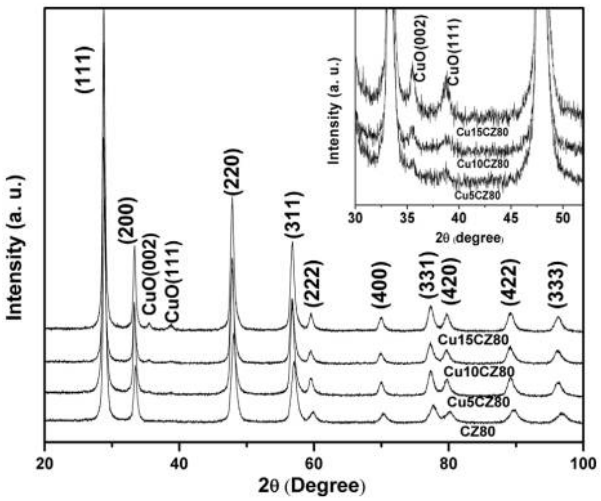

Figure 3 Powder XRD patterns of pure CZ80 and the different Cu-loaded CZ80 oxides. Inset shows the expanded view of the Cu-region (2Θ = 30°–55°)

show any variation to the nominal Ce–Zr support, the absence of segregated Cu-containing particles at the surface of the Ce–Zr support points to the incorporation of a part of copper into the Ce–Zr lattice. This result is in agreement with the XPS data, which showed an impressive high copper dispersion. It is also to be noted that the XRD analyses (see inset of Fig. 2) reveal formation of highly dispersed CuO on CZ80 support in all the Cu-loaded CZ80 samples.

In general view (image not included), the structure of the sample with the highest Cu loading, Cu15CZ80, is essentially identical to the lower Cu-loaded sample. However, in this case, several isolated CuO particles can be recognized, as it is shown in its high-resolution image in Fig. 4*c* in accordance with XRD data. These CuO particles are about 4–5 nm in size.

The HRTEM images of the aged (after MSR in the microreactor) samples show the presence of metallic copper (see Fig. 4*d* and *e*). This is in accordance with the *in situ* XPS experiment (see Fig. 2) and also the *ex situ* characterization by XRD (see Fig. 4*f* that shows the XRD of the aged samples spanning the Cu-region; the peak at 43.5° corresponds to Cu^0 (111)). HRTEM image of the aged catalyst of Cu10CZ80 (Cu10CZ80aged) shows the presence of particles with high electron contrast (see Fig. 4*d*). These particles show the characteristic lattice fringes of metallic Cu. The Cu nanoparticles measure about 2 nm in diameter.

In the lattice fringe image of the aged sample of Cu15CZ80 (Cu15CZ80aged; see Fig. 4*e*), a well-developed metallic Cu nanoparticle is shown. The size of the metallic Cu nanoparticles in this sample is larger (about 3–4 nm) with respect to the aged Cu10CZ80 catalyst, in accordance with its higher copper loading (see also Fig. 4*f*). For the aged samples, the $CuO(111)/CeO_2(111)$ peak area ratios are similar, 0.025 for Cu10CZ80, and 0.026 for Cu15CZ80. The least-square-refined lattice parameters of Cu10CZ80aged and Cu15CZ80aged samples are found to be 5.376 (1) Å and 5.375 (1) Å, respectively, which are again similar to the respective as-prepared samples. It is thus not possible to infer on the existence of ionically substituted copper species in the Ce–Zr support in the aged samples, so the existence of Cu^{2+} in the Ce–Zr lattice cannot be completely ruled out.

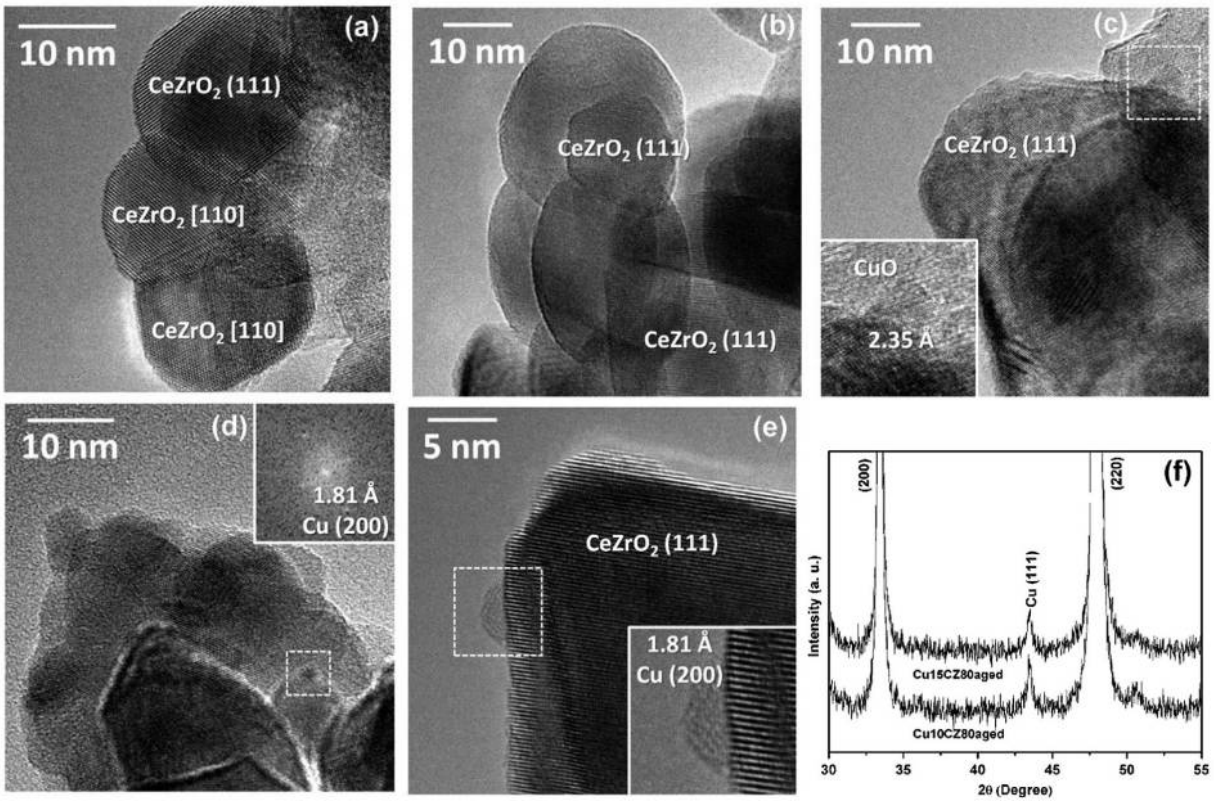

Figure 4 HRTEM images of (a) pure CZ80, (b) Cu10CZ80, (c) Cu15CZ80, (d) Cu10CZ80aged, (e) Cu15CZ80aged, and (f) slow scan XRD data of Cu10CZ80 and Cu15CZ80 catalysts in their aged forms in the 2Θ range 30°–55°

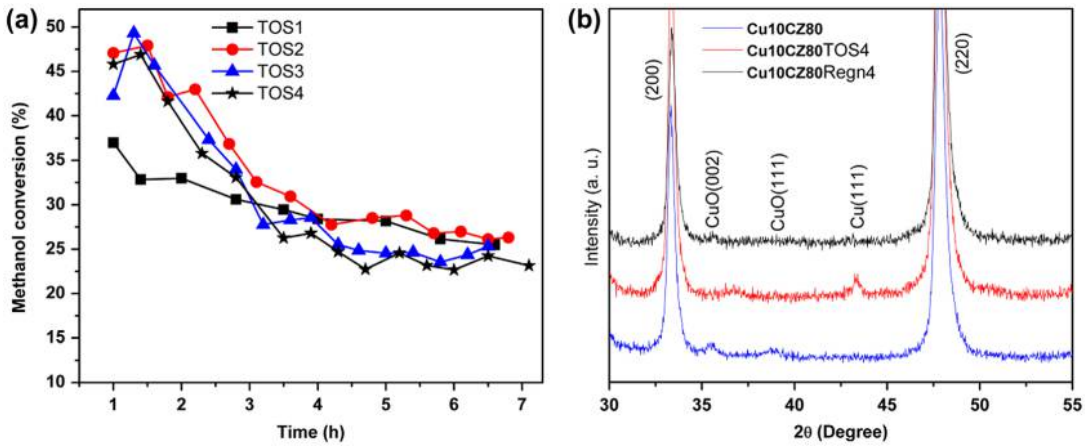

Figure 5 (a) Time-on-stream MSR behavior of Cu10CZ80 catalyst at 250 °C after *in situ* oxidative regeneration treatments for three consecutive cycles (TOS2 to TOS4) along with that in as-prepared form (TOS1) (S/M = 1.1; balance is N_2 in each case to reach a GHSV of 40,000 h^{-1}) and (b) XRD patterns of the samples after the fourth TOS cycle (Cu10CZ80TOS4) and after its *in situ* regeneration (Cu10CZ80Regn4 sample) along with that of the as-prepared sample in the 2Θ range 30°–55°.

As a complementary chemical characterization tool, we have also conducted electron energy loss spectroscopy (EELS) measurements over the Ce–Zr crystallites to check for the presence of substitutional Cu in the Cu10CZ80 catalyst in its as-prepared form. In all cases, the signals of Cu were absent, suggesting that the Ce–Zr crystallites do not contain Cu at all in their structure. It should be stressed out, however, that the sensitivity of Cu to EELS is not very high and that Cu signals are very close to Ce signals, so the fact that we do not see Cu does not necessarily exclude that there is a small amount of Cu in Ce–Zr oxide of the present combustion synthesized catalyst Cu10CZ80.

Now, if we combine the outcomes of XRD, TEM, and EELS studies with the XPS studies of as-prepared and *in situ* MSR-treated samples, it can be proposed that in both the as-prepared samples of Cu10CZ80 and Cu15CZ80, a part of copper is present as finely dispersed CuO (major Cu-phase) on the Ce–Zr support and the rest portion of copper remains as substitutional ions (minor Cu-phase) in the Ce–Zr lattice essentially on the surface layers that is credited to the high Cu-surface concentration obtained for all the as-prepared and regenerated Cu10CZ80 samples. This is a reasonable proposition since combustion synthesis of base and noble-metal-loaded oxide samples is generally composed of a surface solid solution phase containing substitutional metal ion (here copper) sites and the rest of the metal component remains as finely dispersed metal/metal oxide crystallites.[28,29] The reductive MSR atmosphere transforms the oxidized copper species to metallic copper. This is why both the aged catalysts have been characterized to contain copper metal nanocrystallites.

The nature and ratio of the various Cu-related phases and its surface composition decides the on-stream MSR activity pattern. The initial methanol conversion can be correlated to the presence of oxidized copper species—lattice-incorporated Cu^{2+} as well as dispersed Cu^{2+} in the form of CuO on the Ce–Zr support. As the time progresses, both these two types of oxidized copper species are reduced to metallic copper which subsequently undergoes sintering to form larger Cu-metal nanocrystallites. The proportion of the oxidized copper species thus decreases with TOS leaving behind a catalyst surface which is less active for the MSR. Here, we can speculate that the finely dispersed CuO on the surface are reduced at a faster pace than the lattice-incorporated Cu^{2+} surface species. A rapid initial fall in methanol conversion followed by a steady decrease in conversion is thus observed in the on-stream MSR pattern of the Cu10CZ80 and Cu15CZ80 catalysts.

From the TOS tests, it is evident that the initial activity of the Cu15CZ80 catalyst is more than that of the Cu10CZ80 catalyst that can be attributed to the larger loading of copper in the former (6.2 wt-% vs. 4.1 wt-%). But with the progress of reaction, the methanol conversion exhibited by the former catalyst decreases below that of the latter and is associated with a larger amount of CO formation. The deactivation of catalyst is mainly associated with the thermal sintering of the small copper nanoparticles leading to a decrease of the active SA[30–32] and or the reduction of oxidized copper to its metallic form.[3] The phase analyses as well as structural studies have already proved that metallic copper is present in both the aged samples, the size of Cu particles being larger in the higher Cu-loaded sample Cu15CZ80. Owing to the larger loading of copper in it, the extent of sintering is more in Cu15CZ80 than in Cu10CZ80. So, the TOS behavior of the Cu10CZ80 and Cu15CZ80 can be accounted for by noting the reduction of oxidized copper to metallic copper followed by its sintering. The sintering becomes more evident in the second day of test, bringing the TOS conversion values of Cu15CZ80 below that of Cu10CZ80.

A rough estimate of the turnover frequencies (TOFs) of the two finalized catalysts have been calculated by considering the mole of hydrogen produced per mole of total copper (nominal amount taken during synthesis) per second at 250 °C after 1 h of reaction. The TOFs are calculated to be 0.034 and 0.025 s^{-1}, respectively for the Cu10CZ80 and Cu15CZ80 catalysts. We have also calculated the TOF values of the as-prepared and aged samples of Cu10CZ80 by considering the surface concentration of copper from XPS and Cu particle size from HRTEM as reported recently.[25] The TOF values of the

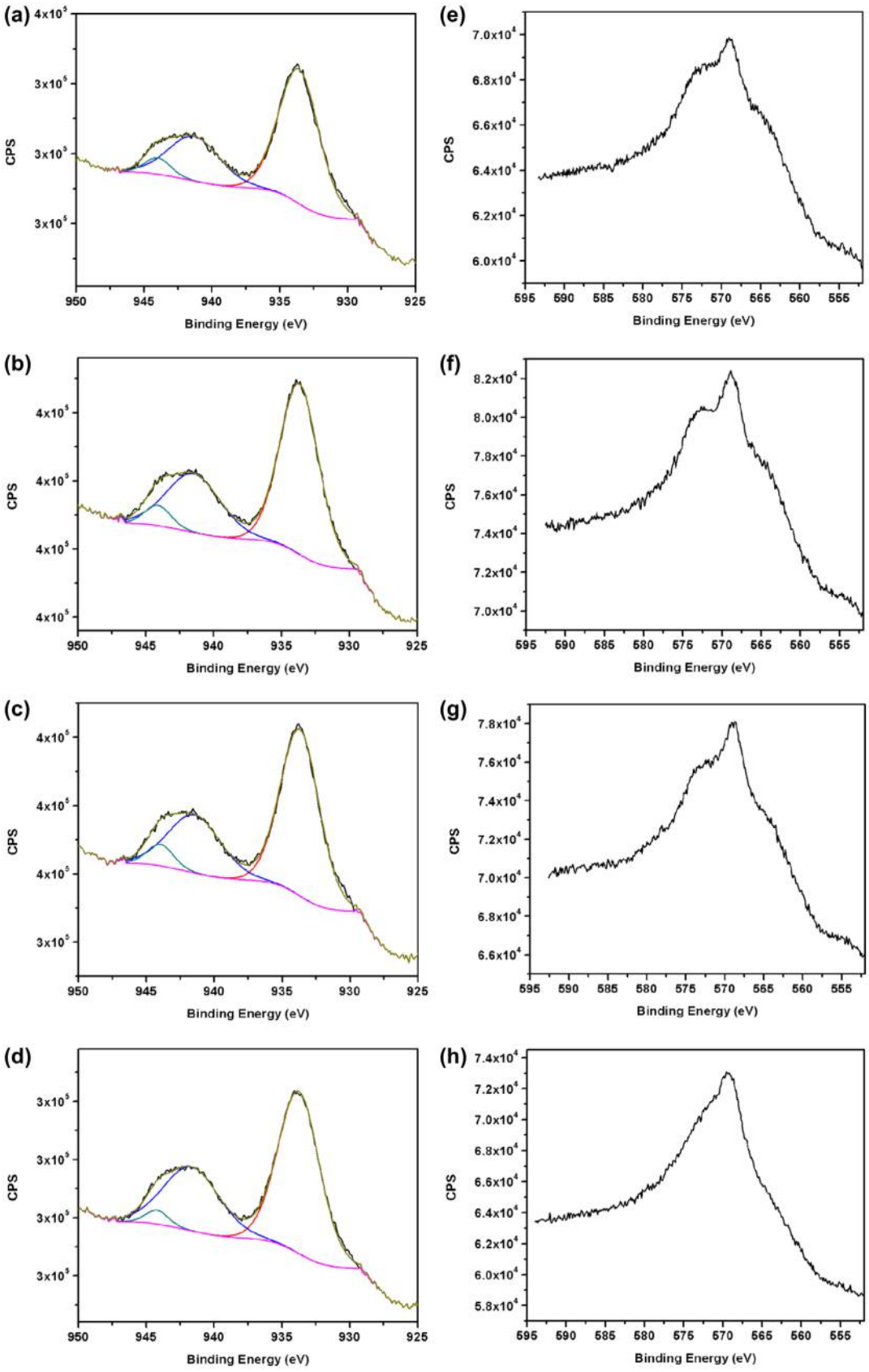

Figure 6 XPS of Cu $2p_{3/2}$ regions of (a) Regn1, (b) Regn2, (c) Regn3, and (d) Regn4 samples of Cu10CZ80; Cu LMM Auger spectra of (e) Regn1, (f) Regn2, (g) Regn3, and (h) Regn4 samples of Cu10CZ80

as-prepared and aged samples calculated thus are 0.15 and 0.16 s^{-1}, respectively.

Finally, we looked into the aspect of regeneration characteristics of Cu10CZ80. After the first cycle of TOS test (at 250 °C

for 6 h; TOS1), the catalyst was purged with nitrogen to RT and left in this flow for overnight and the next day it was regenerated *in situ* in 20% O_2 in N_2 (flowing at 30 mL min^{-1} from RT to 350 °C, at the heating rate of 10 °C min^{-1} and dwell there for 1 h). This was followed by cooling in N_2 to 250 °C and the TOS behavior was assessed again for further 6 h (TOS2). The catalyst was subsequently cooled in nitrogen and left overnight at RT and the cycle of TOS tests was continued in the following days (TOS3 and TOS4). Fig. 5*a* shows the conversion values recorded for the regenerated samples along with the TOS data of the as-prepared sample (reproduced from Fig. 1*b*). The regeneration behavior is quite impressive up to ~4 h showing a higher conversion than recorded over the as-prepared form of the catalyst, beyond which the conversions observed are similar to each other. Thus, the combustion synthesized catalyst of this study can be regenerated easily with an intermediate oxidation treatment. We have already explained the loss in activity during TOS to the formation of Cu^0 followed by sintering based on XRD, HRTEM, and *in situ* XPS findings. In the following texts, we put forward possible explanations for the TOS behavior of the regenerated samples based on XRD and XPS analysis.

We first attempt to explain the TOS behavior recorded for the Cu10CZ80 catalyst on regeneration by analyzing the powder XRD patterns of the sample obtained at the end of these TOS tests (Cu10CZ80TOS4 sample) and the one after its *in situ* regeneration (Cu10CZ80Regn4 sample). Fig. 5*b* shows the XRD patterns (slow scan data) of the Cu region (2θ from 25° to 55°) of these samples along with the as-prepared catalyst. The sample after the fourth cycle of TOS is characterized by Cu^0 presence, as expected. The CuO(111)/CeO_2(111) peak area ratio of this sample (after four consecutive cycles) is calculated to be 0.013 which is half of the aged catalyst after 20 h of TOS. This can be attributed to the presence of finer crystallites of copper in the cycled sample (Cu10CZ80TOS4 sample). Interestingly, for the regenerated sample, no CuO-related diffraction peaks could be identified. Thus, the oxidative treatment generates too small copper species (below the detection limit of XRD) and redistributes them in an efficient manner on the catalyst surface. The least-square-refined lattice parameters of the TOS4 and Regn4 samples remain similar (5.3780(7) Å and 5.3740(1) Å, respectively) to the as-prepared sample that again point to no major structural change due to these treatments.

In order to gain further insights about the surface properties of the Cu10CZ80 catalyst subsequent to regeneration in the microreactor, we have carried out XPS analysis (*ex situ* samples) of all the regenerated samples (Regn1 to Regn4 followed by the catalyst name). Fig. 6*a–d* shows the Cu $2p_{3/2}$ region of all these samples. It is clearly evident that all the regenerated samples are very similar. They exhibit rather constant Cu/(Ce+Zr) atomic ratios (0.19–0.21), except sample Regn4 that is enriched in Cu (exhibiting an atomic ratio of 0.32). On the other hand, it is clear from both the photoemitted electrons and the Auger lines (see Fig. 6*e–h*) that in all the regenerated samples, copper exists only as Cu(II), which nicely fits with the reaction scheme that we have proposed based on the *in situ* MSR studies in the XPS chamber. It should be kept in mind that the samples have been analyzed *ex situ*, so may be the sample contains reduced Cu under reaction conditions (as we saw in the *in situ* MSR experiment) and the surface oxidizes upon exposure to air. We did actually note a visible change in color of the samples (from black to gray, the color of the as-prepared sample) collected after the regeneration tests when exposed to air in the subsequent days which we could not avoid before performing the XPS measurements. This natural tendency of the combustion-made sample to get spontaneously oxidized in air can possibly explain the differences in the Cu atomic percentages obtained from the *in situ* and *ex situ* XPS data of the various Cu10CZ80 samples. The surface Ce/Zr atomic ratio of the regenerated samples maintains the same value of about 4.5 to that of the sample after *in situ* MSR. The surface enriched highly with nanosized copper species is proposed to be responsible for the overall gain in the MSR activity during initial stages (first 4 h of MSR). Afterward, the catalyst surface of the regenerated sample resembles that of the as-prepared sample and thus shows similar reforming activity.

Conclusions

In the present study, we have shown that the solution combustion synthesis is a simple one-step route to prepare Cu-based ceria–zirconia oxides that are active for MSR. The Cu/$Ce_{0.8}Zr_{0.2}O_2$ catalyst (Cu10CZ80) possessing a low SA of 25 $m^2 g^{-1}$ and containing 4.1 wt-% Cu (nominal value) shows the best MSR activity exhibiting a methanol conversion of ~51% at 300 °C when the GHSV is maintained at 40,000 h^{-1}. The copper is present both as substitutional ion (minor Cu-phase) and as dispersed CuO crystallites (major Cu-phase) over ceria–zirconia in the as-prepared catalysts. The loss of activity during on-stream MSR tests (aging treatment) results from the complete reduction of copper followed by its sintering. Introduction of an intermediate *in situ* oxidation step leads to nearly complete regeneration of the MSR behavior in the consecutive TOS cycles of methanol reforming.

Acknowledgments

DD thanks JNMF for a research fellowship. Financial support from the Department of Science and Technology, Government of India, by a grant (SR/S1/PC-28/2010) to AG and DST Special Grant to the Department of Chemistry of Jadavpur University in the International Year of Chemistry 2011 is gratefully acknowledged. AG is grateful to Dr. Parthasarathi Bera of National Aerospace Laboratories, India, for useful discussion. JL is Serra Húnter Fellow and is grateful to ICREA Academia program (Generalitat de Catalunya) and MINECO grant ENE2012-36368.

References

1. D. Ramirez, L. F. Beites, F. Blazquez and J. C. Ballesteros: *Int. J. Hydrogen Energy*, 2008, **33**, (16), 4433–4443.
2. D. R. Palo, R. A. Dagle and J. D. Holladay: *Chem. Rev.*, 2007, **107**, (10), 3992–4021.
3. Y. Choi and H. G. Stenger: *Appl. Catal. B Environ.*, 2002, **38**, (4), 259–269.
4. S. Sá, H. Silva, L. Brandão, J. M. Sousa and A. Mendes: *Appl. Catal. B Environ.*, 2010, **99**, (1–2), 43–57.
5. S. D. Jones, L. M. Neal and H. E. Hagelin-Weaver: *Appl. Catal. B Environ.*, 2008, **84**, (3–4), 631–642.
6. A. Mastalir, B. Frank, A. Szizybalski, H. Soerijanto, A. Deshpande, M. Niederberger, R. Schomäcker, R. Schlögl and T. Ressler: *J. Catal.*, 2005, **230**, (2), 464–475.
7. H. Oguchi, T. Nishiguchi, T. Matsumoto, H. Kanai, K. Utani, Y. Matsumura and S. Imamura: *Appl. Catal. A Gen.*, 2005, **281**, (1–2), 69–73.

8. L. Zhang, L. Pan, C. Ni, T. Sun, S. Zhao, S. Wang, A. Wang and Y. Hu: *Int. J. Hydrogen Energy*, 2013, **38**, (11), 4397–4406.
9. Z. Lei, P. Li-wei, N. Chang-jun, S. Tian-jun, W. Shu-dong, H. Yong-kang, W. An-jie and Z. Sheng-sheng: *J. Fuel Chem. Technol.*, 2013, **41**, (7), 883–888.
10. A. Haghofer, K. Föttinger, F. Girgsdies, D. Teschner, A. K. Knop-Gericke, R. Schlögl and G. Rupprechter: *J. Catal.*, 2012, **286**, 13–21.
11. M. Behrens, S. Zander, P. Kurr, N. Jacobsen, J. Senker, G. Koch, T. Ressler, R. W. Fischer and R. Schlögl: *J. Am. Chem. Soc.*, 2013, **135**, (16), 6061–6068.
12. R. Figueiredo, A. Marťinez-Arias, M. Granados and J. L. Fierro: *J. Catal.*, 1998, **178**, (1), 146–152.
13. L. C. Wang, Y. M. Liu, M. Chen, Y. Cao, H. Y. He, G. S. Wu, W. L. Dai and K. N. Fan: *J. Catal.*, 2007, **246**, (1), 193–204.
14. J. Agrell, H. Birgersson, M. Boutonnet, I. Melián-Cabrera, R. M. Navarro and J. L. G. Fierro: *J. Catal.*, 2003, **219**, (2), 389–403.
15. H. Jeong, K. Kim, T. Kim, C. Ko, H. Park and I. Song: *J. Power Sources*, 2006, **159**, (2), 1296–1299.
16. X. Zhang and P. Shi: *J. Mol. Catal. A Chem.*, 2003, **194**, (1–2), 99–105.
17. R. Maache, R. Brahmi, L. Pirault-Roy, S. Ojala and M. Bensitel: *Top. Catal.*, 2013, **56**, (9–10), 658–661.
18. B. A. Peppley, J. C. Amphlett, L. M. Kearns and R. F. Mann: *Appl. Catal. A Gen.*, 1999, **179**, (1–2), 31–49.
19. H. Purnama, T. Ressler, R. E. Jentoft, H. Soerijanto, R. Schlögl and R. Schomäcker: *Appl. Catal. A Gen.*, 2004, **259**, (1), 83–94.
20. X. K. Gu and W. X. Li: *J. Phys. Chem. C*, 2010, **114**, (49), 21539–21547.
21. A. Szizybalski, F. Girgsdies, A. Rabis, Y. Wang, M. Niederberger and T. Ressler: *J. Catal.*, 2005, **233**, (2), 297–307.
22. H. Oguchi, H. Kanai, K. Utani, Y. Matsumura and S. Imamura: *Appl. Catal. A Gen.*, 2005, **293**, 64–70.
23. C. Pojanavaraphan, A. Luengnaruemitchai and E. Gulari: *Appl. Catal. A Gen.*, 2013, **456**, 135–143.
24. C. Pojanavaraphan, A. Luengnaruemitchai and E. Gulari: *Int. J. Hydrogen Energy*, 2013, **38**, (6), 1384–1362.
25. D. Das, J. Llorca, M. Dominguez, S. Colussi, A. Trovarelli and A. Gayen: *Int. J. Hydrogen Energy*, 2015, **40**, (33), 10463–10479.
26. E. Moretti, L. Storaro, A. Talon, M. Lenarda, P. Riello and R. Frattini: *Appl. Catal. B Environ.*, 2011, **102**, (3–4), 627–637.
27. M. Abdullah and K. Khairurrijal: *J. Nano Saintek.*, 2008, **1**, (1), 28–32.
28. M. S. Hegde, G. Madras and K. C. Patil: *Acc. Chem. Res.*, 2009, **42**, (6), 704–712.
29. P. Bera, K. R. Priolkar, P. R. Sarode, M. S. Hegde, S. Emura, R. Kumashiro and N. P. Lalla: *Chem. Mater.*, 2002, **14**, (8), 3591–3601.
30. B. Frank, F. C. Jentoft, H. Soerijanto, J. Kröhnert, R. Schlögl and R. Schomäcker: *J. Catal.*, 2007, **246**, (1), 177–192.
31. M. Kurtz, H. Wilmer, T. Genger, O. Hinrichsen and M. Muhler: *Catal. Lett.*, 2003, **86**, (1/3), 77–80.
32. M. V. Twigg and M. S. Spencer: *Top. Catal.*, 2003, **22**, (3/4), 191–203.